Identification of a Quasiseparatrix Layer in a Reconnecting Laboratory Magnetoplasma

Eric E. Lawrence* and Walter Gekelman†

Department of Physics and Astronomy, University of California, Los Angeles, Los Angeles, California 90095, USA

(Received 24 May 2009; published 3 September 2009)

The concept of quasiseparatrix layers (QSLs) has emerged as a powerful tool to study the connectivity of magnetic field lines undergoing magnetic reconnection in solar flares. Although they have been used principally by the solar physics community until now, QSLs can be employed to shed light on all processes in which reconnection occurs. We present the first application of this theory to an experimental flux rope configuration. The three-dimensional data set acquired in this experiment makes the determination of the QSL possible.

DOI: 10.1103/PhysRevLett.103.105002 PACS numbers: 52.35.Vd, 52.35.Py

Magnetic field line reconnection is still considered, by some, to be one of the most important topics in plasma physics. It has been in this category for close to 30 years. Many early [1–5] as well as recent [6,7] reconnection experiments forced magnetic flux to merge and form X points or a neutral sheet. In nature, reconnection can occur when fields are entrained in flows, such as in the magnetotail [8], or when magnetic field is locked into highly conducting boundaries, such as in solar footprints [9]. The source of all magnetic fields in a plasma are current systems, although in experiments some of the current can be in conductors entrained in the plasma. From this perspective it is obvious that reconnection can occur in dynamic current systems. For example, reconnection has been observed in three-dimensional current systems in the aftermath of a collision of two dense plasmas in a background plasma [10]. In the Sun, coronal mass ejections can lead to flux ropes [11] that emerge from the corona and can reach Earth. They may remain anchored on the Sun, or break away to become plasmoids [12]. A single flux rope carries a current which makes the magnetic field surrounding it helical. Two or more adjacent flux ropes can interact via their $\mathbf{J} \times \mathbf{B}$ force. This may lead to merging as was seen in an early experiment [13] in which the process lead to a force free state where the magnetic fields and plasma currents became parallel. A recent experiment using washer stack guns to produce initially parallel current carrying plasmas showed that magnetic field reconnection occurs when two flux ropes merge [14].

In 2D reconnection theory, regions of unconnected magnetic field lines are bounded by lines called magnetic separatrices where the magnetic topology changes discontinuously. At points or lines where the magnetic field vanishes, field lines can break and reconnect, releasing magnetic energy. However, in 3D, reconnection is possible in the absence of separatrices. Instead, one can define a generalization of a separatrix called a quasiseparatrix layer (QSL) [15]. At a QSL, the field connectivity changes rapidly but continuously across a narrow spatial region. QSLs have proven extremely useful in identifying regions of 3D magnetic reconnection in theoretical configurations [16] and in observations of solar flares [17,18]. In particular, the geometry of the layer is that of a hyperbolic flux tube (HFT) [16], which is thought to be a preferred site for current layer formation [19–21].

Here we report fully three-dimensional reconnection where two flux ropes are immersed in a magnetoplasma capable of sustaining Alfvén waves. Data were acquired at 20 000 spatial locations and as a function of time. The volumetric data set allows the reconstruction of field lines as well as the three-dimensional current system that evolves. This in turn allows one to observe, for the first time in an experiment, a QSL.

This experiment was conducted in the Large Plasma Device (LAPD) at UCLA. The background plasma is cylindrically shaped with a length of 17 m and a diameter of 60 cm. It is formed by a pulsed 1 Hz dc discharge from a barium oxide-coated nickel cathode. A molybdenum anode is 30 cm from the cathode, and the column is terminated by a floating mesh, so no net current is present in the background plasma. For this experiment, a helium plasma is produced with parameters $n \sim 2.5 \times 10^{12}$ cm^{-3}, $T_e \sim 5$ eV, $T_i \sim 1$ eV, and $B_{z0} \sim 270$ G.

To create the flux ropes, two current channels inside the background plasma are produced by directly-heated lanthanum hexaboride (LaB_6) cathodes mounted on a movable shaft. A schematic of the experimental layout is shown in Fig. 1. The cathodes are constructed by cutting 1 mm ($0.15\rho_i$) slits into a 2.6 cm $\times$ 2.6 cm slab of LaB_6 to form a serpentine shape. A dc power supply provides 570 W of direct heating to maintain the 1800 °C cathode temperature.

The LaB_6 cathodes are located at $z = 0$ cm (facing and 1400 cm away from the main cathode). The upper and lower cathodes are positioned in this axial plane at (x, y) coordinates (0.0, 8.0) cm and (0.0, 4.3) cm, respectively. A 16.5 cm circular molybdenum mesh anode is installed at $z = 900$ cm. The cathodes are biased at 100 V with respect to this anode via a transistor-switched capacitor bank. Each cathode emits 30 A.

The LaB_6 cathodes are pulsed for 2 ms during the active phase of the 14 ms background plasma discharge. Typical

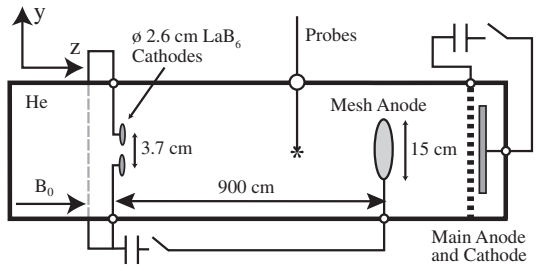

FIG. 1. Schematic of experiment (not to vertical scale). The background He plasma is produced by a BaO coated cathode that is biased to a mesh anode by a transistor-switched capacitor bank. The LaB_6 cathodes, pulsed by a separate capacitor bank, produce the flux ropes.

discharge currents for the LaB_6 cathodes are shown in Fig. 2. The characteristic rise time for the LaB_6 currents is 10 μs. For about 500 μs, the currents are relatively quiescent, but eventually a strong coherent oscillation appears. Note that the round-trip Alfvén transit time, τ_A, is approximately 100 μs inside the current channels.

To diagnose the plasma, 3-axis magnetic ($\dot{B}$) probes are installed at various axial locations. Each probe is movable in the transverse plane by computer controlled stepper motors. The plasma is highly reproducible, so a data set can be constructed with an ensemble of many shots (sampled at 25 MHz). Two such time series are shown in Fig. 2. The period of these oscillations is 190 μs and is constant across the column, but the amplitude is much stronger at the far end of the column.

The resulting magnetic field lines have a flux rope geometry. Each rope has both writhe and twist components of 180° and 180–270°, respectively. Twist varies somewhat with radius. Data collected from a single current channel configuration show only a twist component. The radius of each rope, defined by the location where $B_\perp$ is at a maximum, is $a = 1.5$ cm. A current carrying cylindrical plasma is predicted to be kink unstable if the Kruskal-Shafranov stability factor $q \equiv 2\pi a B_z / L B_\theta(a)$ is less than 1 [22], where a is as defined above, and L is the length of the plasma. In this experiment, $q \approx 0.7$, so this helical structure is consistent with a kink instability. Representative field lines at $r = 0.5$ cm are shown in Fig. 3(a).

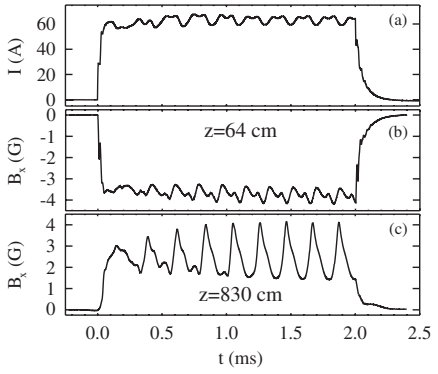

FIG. 2. (a) Typical current in LaB_6-mesh anode circuit. (b) B_x at (0.0, 2.7, 64) cm, which is at the edge of the lower flux rope, and (c) (− 1.5, 9.9, 830) cm, showing pulses due to the rotation of the flux ropes at the far end.

The current density is calculated from Ampère's law, $\mathbf{J} = (c/4\pi)\nabla \times \mathbf{B}$. Typical J_z profiles are shown in Fig. 3(b). The character of the current channels near the cathode does not change appreciably in time, but at the far end of the channels, the profile changes from a merged configuration to a complex filamented one with reverse current layers inside it. The reverse current layers, signatures of magnetic reconnection, are observed for $z \gtrsim 600$ cm.

The flux ropes rotate about their central axes with a rotation period of 190 μs, presumably due to the presence of a parallel plasma flow [23]. Mach probe measurements estimate that $v_z/v_{A\perp} \approx 2$, where $v_{A\perp}$ is the local Alfvén speed, $B_\perp/\sqrt{4\pi\rho}$. The rotation of the field line at the center of each flux rope in the $z = 600$ cm can be seen in the hodograms in Fig. 4(a). Figure 4(b) shows the rotation in the $z = 830$ cm plane, where each rope sweeps out a larger area as it rotates.

The perpendicular separation Δs between the central field lines at $z = 600$ cm and $z = 830$ cm is shown in Fig. 4(c). At $z = 600$ cm, we can see that the field lines maintain a relatively constant separation, but at $z = 830$ cm there are 2 times where Δs decreases quickly.

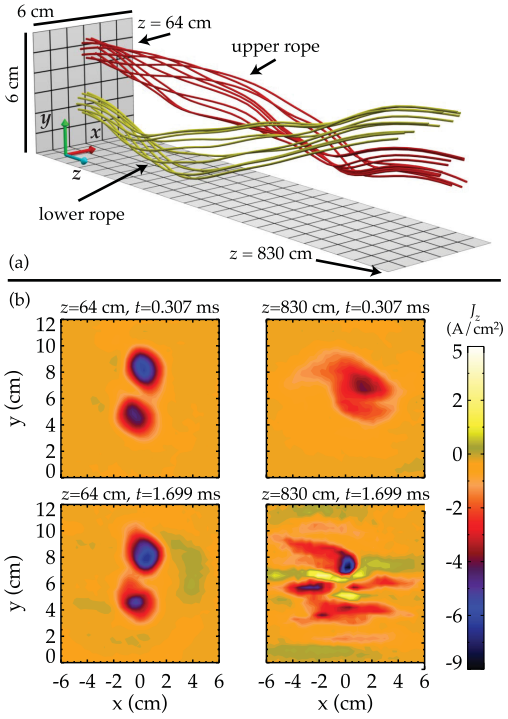

FIG. 3 (color). (a) Two sets of representative field lines at $t = 1.615$ ms. The field lines are seeded from a 1.0 cm diameter circle centered at each current channel in the $z = 64$ cm plane. The axial dimension is compressed 30 times. (b) J_z at each end plane at an early time (top row) and at a late time (bottom row) in the discharge.

These times correspond to the positions on the hodograms indicated by diamonds ($t = 1.699$ ms) and circles ($t = 1.790$ ms). During these times when the flux ropes are colliding, the reverse current sheets are present, and one expects magnetic reconnection as flux piles up.

To determine the location of the QSLs, we calculate the squashing degree [16]. Consider two transverse planes at $z = z_0$ and $z = z_1$. Each field line that intersects the $z = z_0$ plane at coordinates (x, y) has corresponding points $(X(x, y), Y(x, y))$ where it intersects the $z = z_1$ plane. The squashing degree,

$$Q = \frac{(\frac{\partial X}{\partial x})^2 + (\frac{\partial X}{\partial y})^2 + (\frac{\partial Y}{\partial x})^2 + (\frac{\partial Y}{\partial y})^2}{|B_z(z_0)/B_z(z_1)|},$$

indicates how much the endpoints in the z_1 plane change relative to small movements in the z_0 plane. Regions where $Q \gg 2$ define QSLs. In this experiment, $|1 - B_z(z_0)/B_z(z_1)| \lesssim 0.005$, so we neglect this term in our calculations. Q does not change if we switch the initial and final planes, so we can assign a value of Q to each field line.

In order to accurately compute field lines, the magnetic field data set must be divergenceless to a high degree of precision, and preferably described analytically by a set of splines. Nonzero divergence can be introduced from measurement errors such as small misalignment of the probe head, or even by interpolation between grid points. We follow the procedure described in detail in [24] to "divergence clean" the data set. Briefly, **B** is integrated in Fourier space to find the magnetic vector potential **A**, which is then fitted with tricubic splines. The splines are then differentiated analytically to get the divergenceless magnetic field.

To compute Q, we seed field lines at $z = 64$ cm and determine where they intersect the $z = 830$ cm plane. The field line starting and end points are calculated on a numerical grid with 4500×5100 points with 9.33×10^{-4} cm spacing. The derivatives of the mappings of x and y coordinates between each plane then provide Q. This assigns a value of Q to every field line starting in the $z = 64$ cm plane. The numerical grid is considerably finer than the measurement grid, but Q is primarily a function of the global structure of the magnetic field. Calculation of Q on coarser grids shows similar distributions, but the peaks of Q are not as well resolved.

A plot of $\log_{10}(Q)$ in this plane during the first colliding phase ($t = 1.699$ ms) is shown in Fig. 5. The "S" shape of the QSL is quite similar to what has been observed in simulations of merging twisted flux tubes [25]. The S actually consists of several layers stacked together, similar to the fine double peaks found in the analytical configuration in [26].

At other times, the Q distribution has a similar overall profile, but the layers within the S move around and their peak values of Q change. We find that $Q(t)$ attains local maxima when Δs reaches local minima; in other words, the field lines are most diverged during flux rope collisions.

Since Q is strongly peaked, we can visualize the QSL by plotting the surface composed of field lines with Q greater than some threshold; here we select $Q = 1000$ to visualize the most salient features of the Q distribution. In Fig. 6(a), the $Q = 1000$ surface is shown threading between the two flux ropes. The ends of this surface have a thin profile, but the middle is shaped like an equilateral triangle.

The connectivity of field lines on this surface show that it has a HFT geometry where field lines that are closely spaced at one end of the tube diverge hyperbolically at the other end. In Fig. 6(b) we seed red and yellow field lines at $z = 64$ cm, the top and bottom sides of the QSL, respectively. They are initially separated by the QSL width of

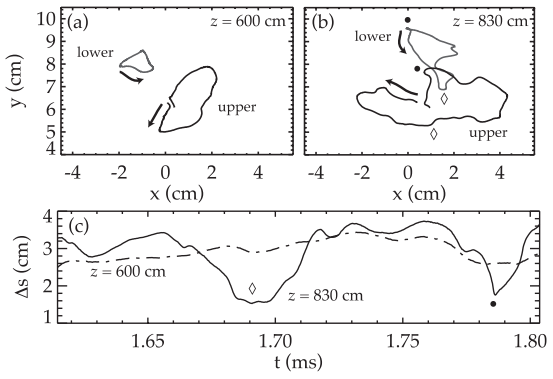

FIG. 4. Hodograms of the point at which the central field line in each flux rope intersects (a) the $z = 600$ cm plane and (b) the $z = 830$ cm plane. "Upper" and "lower" indicate which cathode the field line is seeded from. Each arrow indicates the start of the hodogram at $t = 1610$ ms. (c) Distance Δs between each flux rope at each axial position.

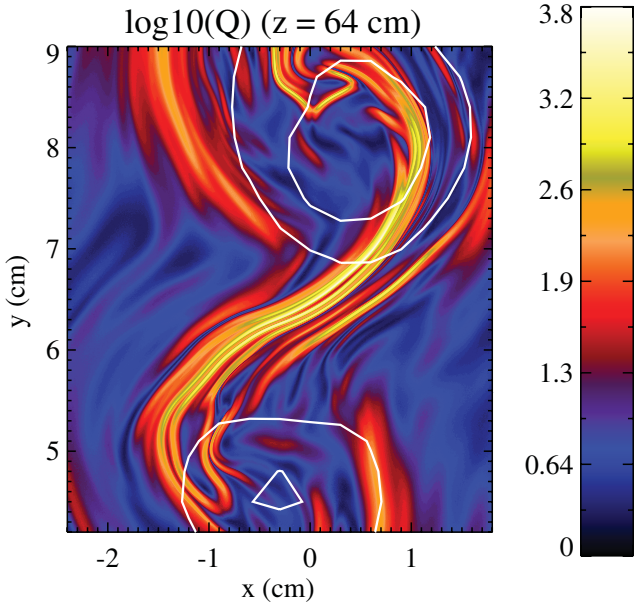

FIG. 5 (color). A logarithmic plot of the squashing degree Q in the $z = 64$ cm plane at $t = 1.699$ ms. Isocontours of $J_z = \{-5.5, -3.0\}$ A/cm^2 are overplotted in white.

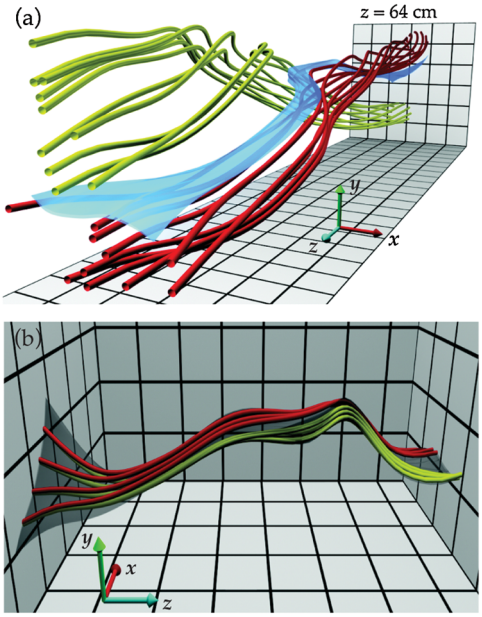

FIG. 6 (color). (a) Representative field lines from each flux rope with the $Q = 1000$ surface in blue threading between them at $t = 1.699$ ms. The field lines are seeded from the same locations as in Fig. 3. The axial dimension is compressed 30 times. (b) A view of the QSL and its hyperbolic flux tube structure. Field lines in red and yellow are seeded from the upper and lower sides of the QSL, respectively. Each pair of field lines is initially separated by the QSL width, 0.05 cm, but diverge to either corner of the QSL (~2 cm separation) in the $z = 830$ cm plane. The axial dimension is compressed 100 times.

0.05 cm, but map to the corners of the QSL at the $z = 830$ cm plane. Here, their separation is approximately 2 cm. Not shown in the figure are the field lines starting at the corners of the QSL at $z = 64$ cm; they map to the wide edges of the QSL in the $z = 830$ cm plane. The QSL generally follows the location of the reverse current sheet, as is expected from a HFT, although the agreement is not exact. We plan to make more detailed comparisons in a future work.

In conclusion, we have experimentally observed a QSL with HFT geometry between magnetic flux ropes. The QSL shape has remarkable similarity to simulations in [25]. A more general theory of 3D reconnection based on QSLs has been put forth [27], and work is being done to apply it to this experiment. It is hoped that, once this theory is fully developed, quantities such as the reconnection rate and current layer thickness can be predicted from the strength and size of the QSLs. This experiment is well suited to help guide and verify these theories.

We thank Vyacheslav Titov for helpful discussions, and Zalton Lucky and Marvin Drandell for providing technical expertise. The work was done at the Basic Plasma Science Facility at UCLA, which is supported by a cooperative agreement between the National Science Foundation and the Department of Energy.

*lawrence@physics.ucla.edu
†gekelman@physics.ucla.edu

[1] R. L. Stenzel and W. Gekelman, J. Geophys. Res. **86**, 649 (1981).
[2] W. Gekelman, R. L. Stenzel, and N. Wild, J. Geophys. Res. **87**, 101 (1982).
[3] R. L. Stenzel, W. Gekelman, and N. Wild, J. Geophys. Res. **87**, 111 (1982).
[4] W. Gekelman and R. L. Stenzel, J. Geophys. Res. **89**, 2715 (1984).
[5] W. Gekelman and H. Pfister, Phys. Fluids **31**, 2017 (1988).
[6] J. Egedal, A. Fasoli, and J. Nazemi, Phys. Rev. Lett. **90**, 135003 (2003).
[7] M. Yamada, H. Ji, S. Hsu, T. Carter, R. Kulsrud, N. Bretz, F. Jobes, Y. Ono, and F. Perkins, Phys. Plasmas **4**, 1936 (1997).
[8] P. D. Henderson, C. J. Owen, I. V. Alexeev, J. Slavin, A. N. Fazakerlay, E. Lucek, and H. Rème, Ann. Geophys. **24**, 651 (2006).
[9] J. Chen, J. Geophys. Res. **101**, 27 499 (1996).
[10] W. Gekelman, S. Vincena, and A. Collette, IEEE Trans. Plasma Sci. **36**, 1122 (2008).
[11] J. Chen, R. A. Howard, G. E. Brueckner, R. Santoro, J. Krall, S. E. Paswaters, O. C. St. Cyr, R. Schwenn, P. Lamy, and G. M. Simnett, Astrophys. J. Lett. **490**, L191 (1997).
[12] J. T. Gosling, in *Physics of Magnetic Flux Ropes*, edited by C. T. Russell, E. R. Priest, and L. C. Lee, Geophysical Monograph Vol. 58 (AGU, Washington, DC, 1990), p. 343.
[13] W. Gekelman, J. Maggs, and H. Pfister, IEEE Trans. Plasma Sci. **20**, 614 (1992).
[14] T. P. Intrator, X. Sun, G. Lapenta, L. Dorf, and I. Furno, Nature Phys. **5**, 521 (2009).
[15] E. R. Priest and P. Démoulin, J. Geophys. Res. **100**, 23 443 (1995).
[16] V. S. Titov, G. Hornig, and P. Démoulin, J. Geophys. Res. **107**, 1164 (2002).
[17] C. H. Mandrini, P. Démoulin, L. Driel-Gesztelyi, B. Schmieder, G. Cauzzi, and A. Hofmann, Sol. Phys. **168**, 115 (1996).
[18] L. G. Bagalá, C. H. Mandrini, M. G. Rovira, and P. Démoulin, Astron. Astrophys. **363**, 779 (2000).
[19] V. S. Titov, K. Galsgaard, and T. Neukirch, Astrophys. J. **582**, 1172 (2003).
[20] K. Galsgaard, V. S. Titov, and T. Neukirch, Astrophys. J. **595**, 506 (2003).
[21] G. Aulanier, E. Pariat, and P. Démoulin, Astron. Astrophys. **444**, 961 (2005).
[22] J. Freidberg, *Ideal Magnetohydrodynamics* (Plenum Press, New York, 1987).
[23] D. D. Ryutov, I. Furno, T. P. Intrator, S. Abbate, and T. Madziwa-Nussinov, Phys. Plasmas **13**, 032105 (2006).
[24] F. Mackay, R. Marchand, and K. Kabin, J. Geophys. Res. **111**, A06205 (2006).
[25] L. J. Milano, P. Dmitruk, C. H. Mandrini, D. O. Gómez, and P. Démoulin, Astrophys. J. **521**, 889 (1999).
[26] V. S. Titov, Z. Mikic, J. A. Linker, and R. Lionello, Astrophys. J. **675**, 1614 (2008).
[27] V. S. Titov, T. G. Forbes, E. R. Priest, Z. Mikić, and J. A. Linker, Astrophys. J. **693**, 1029 (2009).